



Sampling below the Nyquist density using spectral subtiles

ROBERT J. MARKS II^{1,2} ¹Department of Electrical and Computer Engineering, Baylor University, Waco, Texas 76706, USA (Robert_Marks@Baylor.edu)²Walter Bradley Center for Natural and Artificial Intelligence, Dallas, Texas 76706, USA

Received 5 March 2019; revised 13 May 2019; accepted 10 June 2019; posted 11 June 2019 (Doc. ID 361668); published 11 July 2019

An image is assumed to have a spectrum zero outside of a defined support. To avoid aliasing, the replicated support due to sampling cannot overlap. The minimum sampling density corresponding to nonoverlapping supports is the Nyquist density. Replication often necessitate gaps. Support shapes that fill the frequency plane without gaps are tiles. We offer a strategy for achieving minimum sampling density when the spectrum is confined to a subtile. Cookie cutter versions of the subtile shape, when rotated, translated, and/or flipped, result in a tile. The composite signal can have symmetric redundancies that allow reduction of the sampling density to the area of the subtile. We analyze the cases for tiles with twofold point symmetry and mirror symmetry. Two subtiles are required to construct a tile. Threefold, fourfold, and sixfold symmetry is also considered. In the cases considered, the overall sampling density in terms of the samples' required storage is reduced to the area of the support of the subtile. © 2019 Optical Society of America

<https://doi.org/10.1364/JOSAA.36.001322>

1. INTRODUCTION

Shown in Fig. 1 on the left is an image $x(\vec{t}) = x(t_1, t_2)$. We will call this image Ed & Ray. On the right is the average of this image with its 180° rotation of the Ed & Ray image: $y(t_1, t_2) = \frac{1}{2}(x(t_1, t_2) + x(-t_1, -t_2))$. Can we regain the Ed & Ray image exactly by sampling the averaged image on the right at half the sampling density of the original image on the left? The surprising answer is yes if the support of the Fourier transform of the image, e.g., the support of the coherent or optical transfer function, conforms to certain properties [1]. The reason is that if samples of the combined images are taken at the same density, only half the samples of the composite image are required. Because of the symmetry of the combined signals, samples taken of the right-hand plane of the averaged image in Fig. 1 are the same as those taken on the left-hand side of the averaged image.

Indeed, adding various rotations of images can decrease the sampling densities by factors of 2, 3, 4, and 6. Exploring the special cases where this applies is the topic of this paper.

2. FOUNDATION

To avoid aliasing in two-dimensional images, sampling must be performed so there is no overlap in the replicated spectra in the Fourier domain. Overlap results in aliasing upon sample interpolation [3]. A tile is defined as a shape that, when replicated, fills the plane without spaces. Example tiles are rectangles,

parallelograms, and equilateral hexagons. A commonly used shape that does not fill the plane is the circle. Unless the support of the spectrum is a tile, there are undesired gaps in the uniform replications. The Papoulis–Marks–Cheung (PMC) approach [4] to sampling shows that by using a divide-and-conquer approach, the sampling density can always be reduced to the area of the support of the spectrum.

We propose an alternate approach applicable to some cases where the support of the spectrum is on a *subtile*. Subtile shapes, copies of which when appropriately replicated, rotated, and transposed, form a larger tile that can fill the frequency plane without gaps. The act of superimposing the subtile shapes can result in a two-dimensional signal with redundancies in the samples. Because of this redundancy, only a fraction of the samples needs to be stored. Doing so can reduce the overall sampling density to the area of the subtile.

We consider subtiles with twofold, threefold, fourfold, and sixfold symmetry. The twofold symmetries considered are point reflection symmetry and mirror symmetry. In all cases, the sampling density can be reduced to the area of the subtile.

3. PRELIMINARIES

Using standard notation [5–7], the two-dimensional Fourier transform of a two-dimensional image $x(\vec{t}) = x(t_1, t_2)$ is

$$X(\vec{u}) = \int_{\vec{t}} x(\vec{t}) e^{-j2\pi\vec{u}^T\vec{t}} d\vec{t},$$

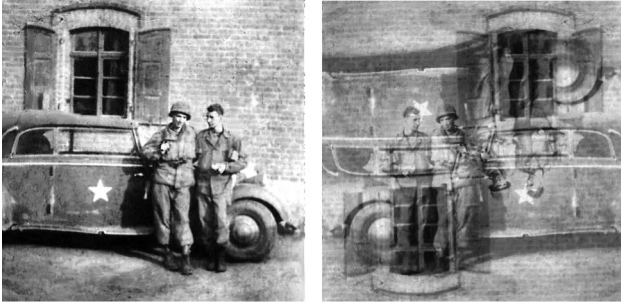


Fig. 1. Ed & Ray image, $x(\vec{t})$, is shown on the left. On the right is the average of the image and its 180° rotation [2]. Photo used with the permission of the author.

where T denotes vector transposition, $\vec{t} = [t_1, t_2]^T$, $\vec{u} = [u_1, u_2]^T$, $d\vec{t} = dt_1 dt_2$, and

$$\int_{\vec{t}} = \int_{t_1} \int_{t_2}.$$

A Fourier transform pair can be written as

$$x(\vec{t}) \leftrightarrow X(\vec{u}).$$

The inverse Fourier transform is

$$x(\vec{t}) = \int_{\vec{u}} X(\vec{u}) e^{j2\pi\vec{u}^T\vec{t}} d\vec{u}.$$

The image $x(\vec{t})$ is real if its spectrum is conjugately symmetric:

$$X^*(-\vec{u}) = X(\vec{u}). \quad (1)$$

When a complex signal is sampled, two real numbers are required to specify a single sample.

When rotated counterclockwise about the origin by an angle of θ , the function $X(\vec{u})$ becomes $X(\mathbf{R}_\theta\vec{u})$, where the rotation matrix is

$$\mathbf{R}_\theta = \begin{bmatrix} \cos(\theta) & \sin(\theta) \\ -\sin(\theta) & \cos(\theta) \end{bmatrix}. \quad (2)$$

Rotating a function on the \vec{t} plane results in its Fourier transform also being rotated by the same angle:

$$x(\mathbf{R}_\theta\vec{t}) \leftrightarrow X(\mathbf{R}_\theta\vec{u}). \quad (3)$$

The Poisson sum formula that couples the replication of spectra in \vec{u} to sampling in \vec{t} is [6]

$$\sum_{\vec{n}} X(\vec{u} - \mathbf{P}\vec{n}) = |\det \mathbf{Q}| \sum_{\vec{n}} x(\mathbf{Q}\vec{n}) e^{j2\pi\vec{u}^T\mathbf{Q}\vec{n}}, \quad (4)$$

where \mathbf{Q} and \mathbf{P} are related by an inverse transpose:

$$\mathbf{Q} = \mathbf{P}^{-T}. \quad (5)$$

A. Periodicity and Sampling Matrices

Let \mathbf{P} denote a 2×2 periodicity matrix with periodicity vectors \vec{p}_1 and \vec{p}_2 :

$$\mathbf{P} = [\vec{p}_1 \ \vec{p}_2].$$

An example of periodicity vectors for hexagonal replication is shown in Fig. 2. If the hexagon apothem is W , then

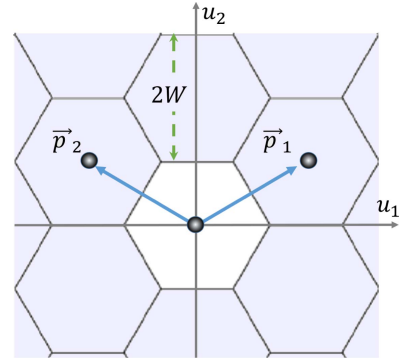


Fig. 2. Unshaded hexagon is replicated. The resulting periodicity vectors are \vec{p}_1 and \vec{p}_2 .

$$\vec{p}_1 = W \begin{bmatrix} \sqrt{3} \\ 1 \end{bmatrix} \quad \text{and} \quad \vec{p}_2 = W \begin{bmatrix} -\sqrt{3} \\ 1 \end{bmatrix},$$

so the periodicity matrix is

$$\mathbf{P} = W \begin{bmatrix} \sqrt{3} & -\sqrt{3} \\ 1 & 1 \end{bmatrix}. \quad (6)$$

The area of a tile is the sampling density. In this case the sampling density is $|\det \mathbf{P}| = 2\sqrt{3}W^2$ samples per unit area.

The sampling matrix \mathbf{Q} specifies the location of the samples in the \vec{t} plane and is related to the periodicity matrix by the inverse transpose in Eq. (5). For the periodicity matrix in Eq. (6), the sampling matrix is

$$\mathbf{Q} = \frac{1}{2W} \begin{bmatrix} \frac{1}{\sqrt{3}} & -\frac{1}{\sqrt{3}} \\ 1 & 1 \end{bmatrix}. \quad (7)$$

The sampling matrix can be interpreted in terms of sampling vectors \vec{q}_1 and \vec{q}_2 :

$$\mathbf{Q} = [\vec{q}_1 \ \vec{q}_2].$$

For the sampling matrix in Eq. (7), the sampling vectors are

$$\vec{q}_1 = \frac{1}{2W} \begin{bmatrix} \frac{1}{\sqrt{3}} \\ 1 \end{bmatrix} \quad \text{and} \quad \vec{q}_2 = \frac{1}{2W} \begin{bmatrix} -\frac{1}{\sqrt{3}} \\ 1 \end{bmatrix}. \quad (8)$$

These vectors, shown in Fig. 3, dictate locations of samples on the \vec{t} plane. Every sample location, shown as dots in Fig. 3, can

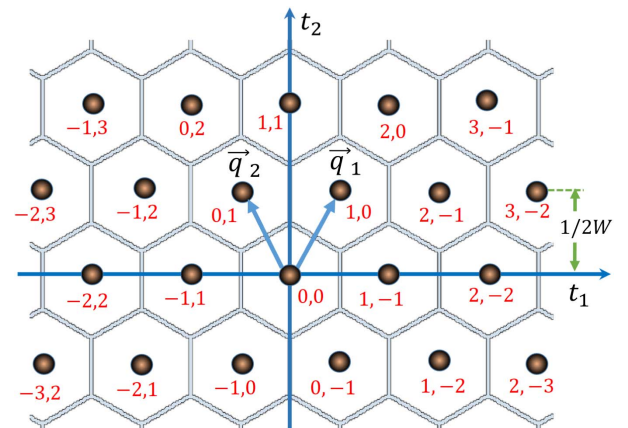


Fig. 3. Sampling vectors \vec{q}_1 and \vec{q}_2 .

be represented as integer weighted sums of the sampling vectors $m_1\vec{q}_1 + m_2\vec{q}_2$ given by

$$\mathbf{Q}\vec{m} = m_1\vec{q}_1 + m_2\vec{q}_2,$$

where m_1 and m_2 are integers and

$$\vec{m} = \begin{bmatrix} m_1 \\ m_2 \end{bmatrix}.$$

For a signal $x(\vec{t})$, the samples corresponding to a sampling matrix of \mathbf{Q} are $x(\mathbf{Q}\vec{m})$. The integer assignments for each sample corresponding to the sampling matrix in Eq. (8) are shown in Fig. 3. The integer pair (3, -1), for example, shows the location of the sample at $3\vec{q}_1 - \vec{q}_2$.

The hexagonal sampling on the \vec{t} plane in Fig. 3 corresponds to the hexagonal spectral replication in the frequency domain in Fig. 2. Note that, on the \vec{u} plane, the flat side of the hexagon is on the top and bottom, while in the \vec{t} plane, the flat sides are on the left and the right.

B. Sampling Theorem

A tile can be replicated over the entire \vec{u} plane with no gaps. If $Y(\vec{u})$ resides in one of the tiles, Fourier transforming the Poisson sum formula in Eq. (4) gives

$$s(\vec{t}) := \sum_{\vec{n}} y(\mathbf{Q}\vec{n})\delta(\vec{t} - \mathbf{Q}\vec{n}) \leftrightarrow |\det \mathbf{P}| \sum_{\vec{n}} Y(\vec{u} - \mathbf{P}\vec{n}),$$

where $|\det \mathbf{P}| = 1/|\det \mathbf{Q}|$, $\delta(\vec{t}) = \delta(t_1)\delta(t_2)$, where $\delta(t)$ is the Dirac delta, and $s(\vec{t})$ is the image of samples. In the Fourier domain, the sum $\sum_{\vec{n}} Y(\vec{u} - \mathbf{P}\vec{n})$ is the unaliased replication over the entire \vec{u} plane. Multiply the Fourier transform of the image of samples in the frequency domain by the mask $F_C(\vec{u}) = |\det \mathbf{Q}|$ inside the tile and zero outside. The corresponding convolution in the \vec{t} domain gives the sampling theorem expression for regaining the image from its samples [6]:

$$y(\vec{t}) = \sum_{\vec{n}} y(\mathbf{Q}\vec{n})f_C(\vec{t} - \mathbf{Q}\vec{n}), \tag{9}$$

where

$$f_C(\vec{t}) \leftrightarrow F_C(\vec{u}).$$

The interpolation function perfectly interpolates, since for any pair of integers k_1 and k_2 in a vector \vec{k} ,

$$f_C(\mathbf{Q}\vec{k}) = \begin{cases} 1 & ; k_1 = k_2 = 0 \\ 0 & ; \text{otherwise} \end{cases}.$$

This relation reduces Eq. (9) to an identity when $\vec{t} = \mathbf{Q}\vec{m}$. We see this interpolation function property in one dimension where the sampling theorem is

$$x(t) = \sum_{n=-\infty}^{\infty} x\left(\frac{n}{2B}\right)\text{sinc}(2Bt - n),$$

where $\text{sinc}(t) = \sin(\pi t)/(\pi t)$ and the spectrum of $x(t)$ is zero outside of the bandwidth support $-B < u < B$. Akin to Eq. (10), the sinc is a perfect interpolation function, because for integer k we have $\text{sinc}(k) = 1$ for $k = 0$ and is otherwise 0.

We can also pass the image of samples through a mask corresponding to a subtile, \mathcal{S} . Define $F_S(\vec{u}) = |\det \mathbf{Q}|$ inside a subtile and zero outside. If, inside the subtile, $Y(\vec{u}) = X(\vec{u})$, then

$$x(\vec{t}) = \sum_{\vec{n}} y(\mathbf{Q}\vec{n})f_S(\vec{t} - \mathbf{Q}\vec{n}), \tag{10}$$

where

$$f_S(\vec{t}) \leftrightarrow F_S(\vec{u}) \tag{11}$$

is the interpolation function. In the \vec{u} plane,

$$F_S(\vec{u}) = \begin{cases} |\det \mathbf{Q}| & ; \vec{u} \in \mathcal{S} \\ 0 & ; \text{otherwise.} \end{cases}$$

Thus,

$$f_S(\vec{t}) = |\det \mathbf{Q}| \int_{\vec{u} \in \mathcal{S}} e^{-j2\pi\vec{u}\vec{t}} d\vec{u}. \tag{12}$$

The function $f_S(\vec{t})$ is not a perfect interpolation function. The sample at one point can contribute to the interpolation at other sample locations.

C. Aliasing

Aliasing can occur when undersampling [8–10] below the Nyquist density. To avoid aliasing, classic sampling theory requires choice of a periodicity matrix \mathbf{P} that replicates a support region so there is no overlap among the replicated spectra. When a support region is a tile, the minimum sampling density occurs when there is maximal packing of the spectral support with no gaps.

As already noted, a circle is not a tile. Maximally packed nonoverlapping circles form a hexagonal pattern that contain gaps. Another gap example is a spectrum confined to an equilateral triangle. Each side of the triangle is of length $2W$. A replication is shown in Fig. 4. No matter what the chosen method of replication, there are significant gaps when overlapping is prohibited. If the triangle is of width $2W$ on all three sides, the hexagonal periodicity matrix for the replication in Fig. 4 is

$$\mathbf{P} = \frac{W}{2} \begin{bmatrix} 3 & -3 \\ \sqrt{3} & \sqrt{3} \end{bmatrix}. \tag{13}$$

The corresponding hexagonal sampling density on the \vec{t} plane in samples per unit area is therefore

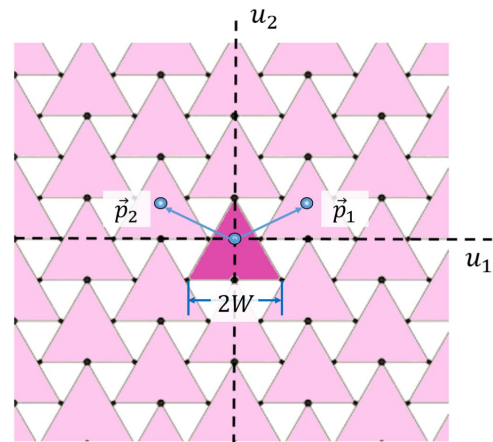


Fig. 4. Spectrum of a two-dimensional signal is zero outside an equilateral triangle. For unaliased sampling, the spectrum must be replicated so there is no overlap. There exists no technique for such replication without gaps.

$$|\det \mathbf{P}| = \frac{3\sqrt{3}W^2}{2}. \quad (14)$$

The PMC approach [4] shows that nonuniform sampling can reduce the overall sampling density to the area of the support of the image spectra. Thus, if the support of an image's spectrum is identically zero outside a circle of radius W , then a sampling density of the corresponding image can be reduced arbitrarily close to πW^2 samples per unit area [11–13]. The PMC approach exploits the required spectral gaps that occur when sampling multidimensional signals. The spectrum is sliced into narrow bands. Each slice is sampled separately. Some bands are zero and do not need to be sampled. By discarding these empty bands, the overall sampling density is reduced ultimately to the area of the support of the spectrum [14]. The PMC approach can be used to reduce the sampling rate for equilateral triangle support to its area $\sqrt{3}W^2$. This is two-thirds of the uniform sampling density in Eq. (14).

4. SAMPLE OVERLAP IN FUNCTIONAL ROTATION

An alternate approach to the PMC approach can apply when the image spectral support is a *subtile*. A subtile is a shape whose multiple copies can be rotated, shifted, and transposed into a tile. These versions of the original image are correspondingly added and sampled. Redundancy of samples of the summed images allows sample decimation. The original subtile image can be reconstructed from the samples remaining.

The subtiles must be such that the samples of the rotated signal lie on top of the samples of the unrotated signal. Consider the signal $x(\vec{r})$. The samples are at $x(\mathbf{Q}\vec{m})$. We now rotate the function to $x(\mathbf{R}_\theta\vec{u})$ and sample using the same sampling matrix \mathbf{Q} . The result is $x(\mathbf{R}_\theta\mathbf{Q}\vec{k})$, where \vec{k} contains only integers. The samples of the rotated signal and the original signal are required to coincide. This happens when

$$\mathbf{Q}\vec{m} = \mathbf{R}_\theta\mathbf{Q}\vec{k}$$

and both \vec{m} and \vec{k} consist of only integers. Equivalently,

$$\vec{m} = \mathbf{Q}^{-1}\mathbf{R}_\theta\mathbf{Q}\vec{k}. \quad (15)$$

If \vec{k} contains only integers, a necessary condition for \vec{m} to contain only integers is that the matrix

$$\mathbf{M} = \mathbf{Q}^{-1}\mathbf{R}_\theta\mathbf{Q} \quad (16)$$

contains only integers.

Often the coinciding of signal samples and the samples of the signal rotations is geometrically obvious. For example, rotating a regular hexagon 60° results in an identical hexagon.

5. TWOFOLD SUBTILES WITH POINT REFLECTION SYMMETRY

Examples of tiles with point reflection symmetry are shown in Fig. 5. Subtiles are shaded. Rotating the subtile 180° about the origin completes the tile.

The equilateral triangle is an example of a subtile of a parallelogram. An equilateral triangle, shown shaded in Fig. 6, is marked t on top and ℓ and r on the left and the right.

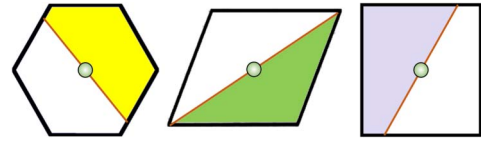


Fig. 5. Tiles with point reflection symmetry: hexagon, parallelogram, and rectangle. Subtiles are shown shaded.

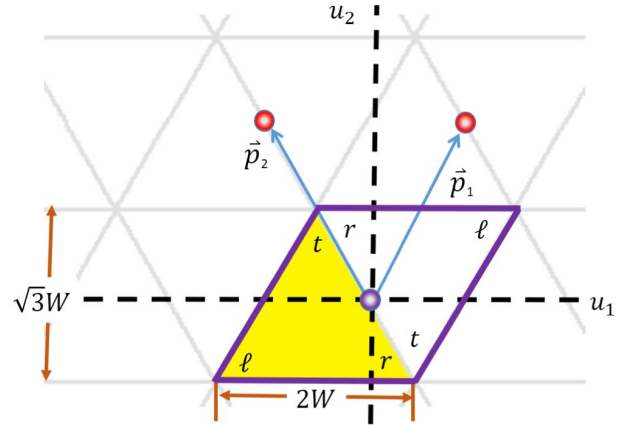


Fig. 6. Triangle support replication.

The triangle is a subtile since it can be flipped to form the parallelogram tile outlined with a bold line. If the image spectrum inside of the shaded triangle is $X(\vec{u})$, then the rotated triangle can be written as $X(\mathbf{R}_{180^\circ}\vec{u})$ where the 180° rotation matrix is

$$\mathbf{R}_{180^\circ} = \begin{bmatrix} -1 & 0 \\ 0 & -1 \end{bmatrix} = -\mathbf{I}. \quad (17)$$

As is the case with any of the point reflection tiles, a tile support is formed by a 180° rotation of the subtile. The image spectrum inside the tile is then

$$Y(\vec{u}) = X(\vec{u}) + X(\mathbf{R}_{180^\circ}\vec{u}) = X(\vec{u}) + X(-\vec{u}). \quad (18)$$

Outside the tile $Y(\vec{u}) = 0$.

A. Sample Redundancy

To reduce the sampling density, advantage is taken of the redundancy of the samples of y . Since

$$x(-\vec{r}) \leftrightarrow X(-\vec{u}),$$

the inverse transform of Eq. (18) is

$$y(\vec{r}) = x(\vec{r}) + x(-\vec{r}). \quad (19)$$

The y image is therefore formed by rotating x by 180° and adding the images. This is illustrated in Fig. 1. The sum is redundant since

$$y(\vec{n}) = y(-\vec{n}). \quad (20)$$

In the example in Fig. 1, the redundancy in the composite image is obvious. Only half the sample needs to be taken. Because of the symmetry of the composite image y , only half the samples are therefore required to define $y(\vec{r})$ and therefore $x(\vec{r})$.

B. Equilateral Triangle Example

For the equilateral triangle subtile shown shaded in Fig. 6, the completed spectrum tile has the support of a parallelogram with periodicity matrix

$$P = \begin{bmatrix} 1 & -1 \\ \sqrt{3} & \sqrt{3} \end{bmatrix} W. \tag{21}$$

The corresponding sampling matrix is

$$Q = P^{-T} = \frac{1}{2W} \begin{bmatrix} 1 & -1 \\ \frac{1}{\sqrt{3}} & \frac{1}{\sqrt{3}} \end{bmatrix}. \tag{22}$$

Because of the symmetry of the samples in Eq. (20), only half the samples $y(Q\vec{n})$ need be stored. Two obvious sampling geometries are shown in Fig. 7. An additional four sampling geometries are in Fig. 8. In all cases, the entire plane is filled

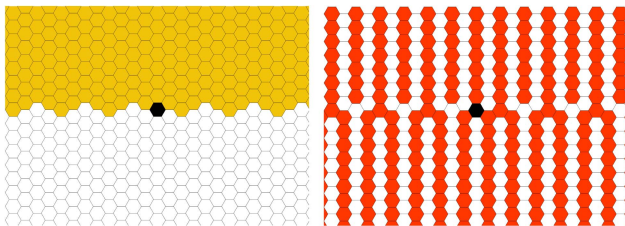


Fig. 7. Two obvious sampling geometries when $y(Q\vec{n}) = y(-Q\vec{n})$, where Q is given in Eq. (22). Left: half plane sampling. Right: vertical sampling. Here and in similar subsequent figures, samples are taken in the middle of each small shaded shape, in this case a hexagon. The origin is colored solid black. The t_1 axis goes to the right and the t_2 axis up.

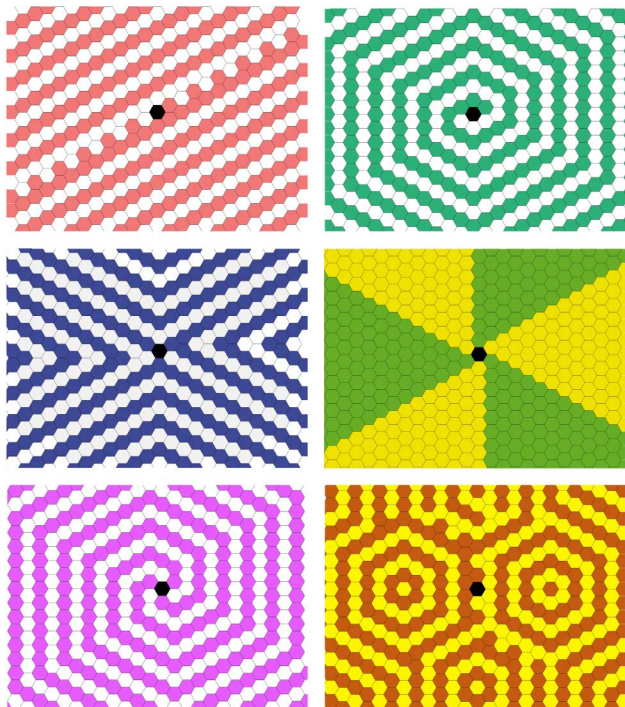


Fig. 8. Six additional sampling geometries when $y(Q\vec{n}) = y(-Q\vec{n})$, where Q is given in Eq. (22). Clockwise from upper left: diagonal, spiral, pie slice, flowers, triple spiral, X geometry.

when the array of samples is rotated 180° and added to the original array.

Since only half the samples are used in the composite image, the sampling density is reduced by a factor of a half to $\sqrt{3}W^2$, which is the area of shaded triangle in Fig. 6.

To find the interpolation function to reconstruct $x(\vec{t})$ from the samples $y(Q\vec{n})$, define the subtile \mathcal{S} on the \vec{u} plane as the shaded equilateral triangle mask in Fig. 6. The interpolation function is then Eq. (12). Then the series in Eq. (10) can be used to regain the function $x(\vec{t})$ from its samples.

C. Summary

Here is a summary. Given an image $x(\vec{t})$ whose spectrum is zero outside the equilateral triangle, the sampling steps are as follows.

- 1) Add the original image to a 180° version of the same image.
 - This forms $y(\vec{t})$ from $x(\vec{t})$ in Eq. (19), as illustrated in Fig. 1.
 - The composite image, $y(\vec{t})$, is redundant in that half of the averaged image can be used to reconstruct the other half.
- 2) Sample the image. Only half the samples need to be stored because of the image’s redundancy.
 - Use the sampling matrix Q in Eq. (22) corresponding to the parallelogram tile shown in Fig. 6.
 - As illustrated in Fig. 1, only half of the samples are needed to define the whole image.
 - Although sampling is performed at high density, only half of the samples need to be stored. The overall sampling density is therefore reduced by a factor of 2.

For restoration:

- 1) Using the redundancy of the composite image, use the known stored samples to fill in those not stored.
- 2) Pass all the samples through a mask (filter) shaped like the equilateral triangle in Fig. 6.
 - The mask is equal to $|\det Q|$ in the equilateral triangle and zero otherwise.
 - In the \vec{t} plane, samples are interpolated using the convolution in Eq. (10).
 - The interpolation function, given in Eq. (12), is weighted by each sample and the results summed. In the traditional 1D sampling theorem, the interpolation function is a sinc [15,16].
- 3) The result is the original image $x(\vec{t})$.
- 4) The sampling density required to restore the image is the area of support, e.g., the area of the triangle.

For the examples to follow, a similar procedure is followed.

D. Relation to Frequency Multiplexing

There is a relationship between subtile sampling and frequency domain multiplexing. Consider the left two images in Fig. 9. The leftmost image is Ed & Ray. The image Toes is in the middle. Assume Ed & Ray’s image spectrum is zero outside the shaded equilateral triangle in Fig. 6 and the Toes image is zero outside the unshaded inverted equilateral triangle that



Fig. 9. On the left is the image of Ed & Ray [2]. This is averaged with the middle image, Toes, to form the averaged image shown on the right. Photo credit for Toes: the author Robert J. Marks II.

completes the parallelogram in Fig. 6 [17]. The two images are therefore block orthogonal in the Fourier domain. This allows sampling of the averaged image shown on the right of Fig. 9 at the Nyquist density dictated by the parallelogram tile support in Fig. 6. From the stored samples, both Ed & Ray and Toes can be individually restored from the samples of the averaged images. The Ed & Ray image is regained by processing all of the samples through the shaded equilateral triangle in Fig. 6. The Toes image results from using the inverted equilateral triangle mask.

In the same sense, for subtile sampling using the 180° rotation, both the original and inverted image can be individually constructed using all of the image samples. Fortuitously, the image samples of the averaged image overlap in such a manner that only half the samples are required.

E. Conjugate Subtile Sampling

A signal whose spectral support is the equilateral triangle in Fig. 6 is necessarily complex. The signal does not comply with the necessary conjugate symmetric requirement in Eq. (1). The composite signal $Y(\vec{u})$ in Eq. (18) is also not conjugately symmetric. The signal $y(\vec{t})$ is therefore also complex.

We can redo the same problem so that the composite image is real and only one number per sample is required. We now show that doing so results in the requirement of the same number of samples per unit area.

Consider again the same equilateral triangle example where, instead of Eq. (18), the *conjugate* of the subtile signal is rotated. In lieu of Eq. (18), define

$$Z(\vec{u}) = X(\vec{u}) + X^*(-\vec{u}). \tag{23}$$

The function Z is now conjugately symmetric:

$$Z(\vec{u}) = Z^*(-\vec{u}).$$

Consequently, $z(\vec{t})$ is real [6]. Since

$$x^*(\vec{t}) \leftrightarrow X^*(-\vec{u}), \tag{24}$$

the inverse Fourier transform of Eq. (23) is

$$z(\vec{t}) = x(\vec{t}) + x^*(\vec{t}) = 2x_{\Re}(\vec{t}), \tag{25}$$

where $x_{\Re}(\vec{t})$ is the real part of $x(\vec{t})$. There is no longer redundancy in samples of $z(\vec{t})$. All samples are now needed to reconstruct $x(\vec{t})$.

We note, though, that the nonconjugated rotation samples in the previous example were complex. Therefore, each sample required two numbers, i.e., the real and imaginary

components. In the current example, real samples are taken using the sampling matrix \mathbf{Q} in Eq. (22) and every sample is required. But since only a single number is required for each real sample, the sampling densities for the two equilateral triangle sampling examples are the same [18].

The original image $x(\vec{t})$ is regained from samples of $z(\vec{t})$ using

$$x(\vec{t}) = \sum_{\vec{n}} z(\mathbf{Q}\vec{n}) f_{\mathcal{S}}(\vec{t} - \mathbf{Q}\vec{n}) = 2 \sum_{\vec{n}} x_{\Re}(\mathbf{Q}\vec{n}) f_{\mathcal{S}}(\vec{t} - \mathbf{Q}\vec{n}),$$

where the interpolation function $f_{\mathcal{S}}(\vec{t})$ is given in Eq. (12). The support \mathcal{S} is the yellow shaded equilateral triangle in Fig. 6.

6. TWOFOLD SUBTILES WITH MIRROR SYMMETRY

Another class of tiles includes those that display mirror symmetry. Examples of tiles with mirror symmetry are shown in Fig. 10. If the spectrum $X(\vec{u})$ is totally contained in the subtile where the u_2 axis acts as the mirror, the completed tile is

$$Y(\vec{u}) = X(u_1, u_2) + X(-u_1, u_2).$$

The inverse Fourier transform is

$$y(t_1, t_2) = x(t_1, t_2) + x(-t_1, t_2).$$

Note the symmetry

$$y(t_1, t_2) = y(-t_1, t_2).$$

A sample of y taken from the right half plane is identical to the mirror sample in the left half plane. Because of the redundancy,

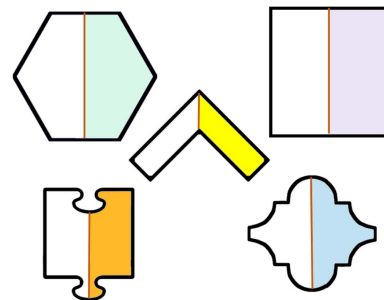


Fig. 10. Four example tiles with mirror symmetry. The subtile for each is shaded.

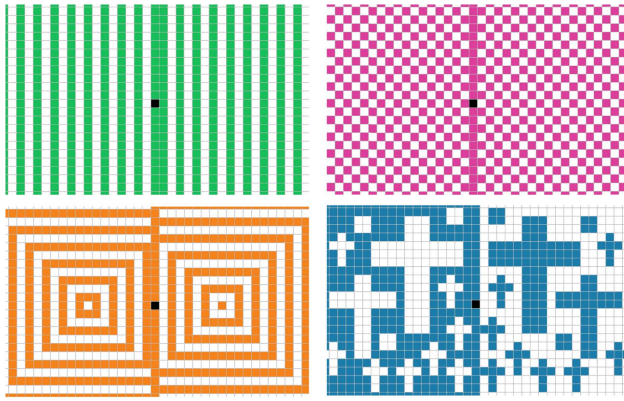


Fig. 11. Four sampling sceneries for twofold mirror symmetry. The bottom right best illustrates the mirroring nature of the sampling geometry.

only one of the samples needs to be stored. Some possible sampling geometries are shown in Fig. 11.

The interpolation function in Eq. (10) is applicable here for the case of the equilateral triangle.

7. FOURFOLD SYMMETRY SUBTILES

The puzzle piece shown shaded in the first quadrant of Fig. 12 is a fourfold symmetric subtile of a square tile. Call the function within this puzzle subtile $X(\vec{u})$. A square tile is formed by adding four versions of the puzzle piece to form

$$Y(\vec{u}) = X(\vec{u}) + X(\mathbf{R}_2\vec{u}) + X(\mathbf{R}_3\vec{u}) + X(\mathbf{R}_4\vec{u}). \quad (26)$$

The rotation matrices, subscripted by quadrants, are

$$\mathbf{R}_2 = \begin{bmatrix} 0 & 1 \\ -1 & 0 \end{bmatrix}; \quad \mathbf{R}_3 = \begin{bmatrix} -1 & 0 \\ 0 & -1 \end{bmatrix}; \quad \mathbf{R}_4 = \begin{bmatrix} 0 & -1 \\ 1 & 0 \end{bmatrix}. \quad (27)$$

Using the notation in Eq. (2),

$$\mathbf{R}_2 = \mathbf{R}_{90^\circ}, \quad \mathbf{R}_3 = \mathbf{R}_{180^\circ}, \quad \mathbf{R}_4 = \mathbf{R}_{270^\circ}.$$

The periodicity matrix for the square tile in Fig. 12 is rectangular,

$$\mathbf{P} = 2W \begin{bmatrix} 1 & 0 \\ 0 & 1 \end{bmatrix},$$

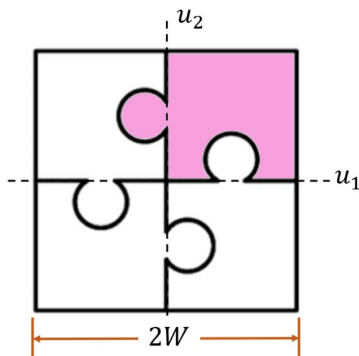


Fig. 12. Four puzzle pieces form a fourfold symmetry.

and the sampling matrix is

$$\mathbf{Q} = \frac{1}{2W} \begin{bmatrix} 1 & 0 \\ 0 & 1 \end{bmatrix}. \quad (28)$$

We note that the \mathbf{M} matrix in Eq. (16) contains all integers for \mathbf{R}_2 , \mathbf{R}_3 , and \mathbf{R}_4 . The samples of all rotated versions of the signal thus coincide. This is trivially obvious from the square sampling geometry. Rotate a square once, twice, or three times and you get a square.

Equivalently, we can write Eq. (26) as

$$Y(u_1, u_2) = X(u_1, u_2) + X(u_2, -u_1) + X(-u_1, -u_2) + X(-u_2, u_1). \quad (29)$$

There is fourfold symmetry in Y :

$$Y(u_1, u_2) = Y(-u_1, u_2) = Y(u_1, -u_2) = Y(-u_1, -u_2).$$

The corresponding inverse transform of Eq. (29) preserves this symmetry:

$$y(t_1, t_2) = x(t_1, t_2) + x(t_2, -t_1) + x(-t_1, -t_2) + x(-t_2, t_1).$$

Specifically,

$$y(t_1, t_2) = y(-t_1, t_2) = y(t_1, -t_2) = y(-t_1, -t_2).$$

Only a fourth of the samples of y are therefore needed. Sampling in a single quadrant is an obvious solution. Sampling geometries are shown in Fig. 13. Only samples in the darker regions are needed. The origin in each case is a black square. The stored samples, when rotated 90° , 180° , and 270° will supply sample values at all points in the plane.

A. Puzzle Piece Conjugate Subtile

Reconsider the same puzzle piece problem in Fig. 12, except conjugation is used to assure conjugate symmetry and therefore a real image. The sampling density can be reduced, but not as much as in the previous example.

In lieu of Eq. (26), define

$$Z(\vec{u}) = X(\vec{u}) + X(\mathbf{R}_2\vec{u}) + X^*(\mathbf{R}_3\vec{u}) + X^*(\mathbf{R}_4\vec{u}), \quad (30)$$

where the rotation matrices are given in Eq. (27). We can rewrite Eq. (30) as

$$Z(u_1, u_2) = X(u_1, u_2) + X(u_2, -u_1) + X^*(-u_1, -u_2) + X^*(-u_2, u_1). \quad (31)$$

Note that

$$Z(\vec{u}) = Z^*(-\vec{u}),$$

so that $z(\vec{t})$ is real. Since

$$x(t_2, -t_1) \leftrightarrow X(u_2, -u_1),$$

we see that

$$2x_{\Re}(t_2, -t_1) \leftrightarrow X(u_2, -u_1) + X^*(-u_2, u_1),$$

so that the inverse Fourier transform of Eq. (31) is

$$z(t_1, t_2) = 2x_{\Re}(t_1, t_2) + 2x_{\Re}(t_2, -t_1). \quad (32)$$

There is no directly useful symmetry as before, but note that Eq. (32) can recursively be written as

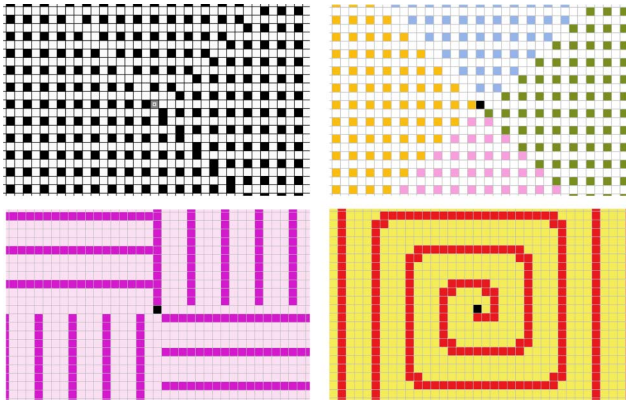


Fig. 13. Some sampling sceneries for the puzzle piece subtile problem in Fig. 12. Samples are taken in the center of the darker or shaded square areas. The origin is shown as a black square. The upper left shows a sampling geometry. The upper right shows the corresponding geometry color coded. The bottom left shows a piecewise linear sampling approach, and the bottom right is a spiral sampling pattern. The sampling matrix for these geometries used the sampling matrix \mathbf{Q} in Eq. (28).

$$\begin{bmatrix} z(t_1, t_2) \\ z(t_2, -t_1) \\ z(-t_1, -t_2) \\ z(-t_2, t_1) \end{bmatrix} = 2 \begin{bmatrix} 1 & 1 & 0 & 0 \\ 0 & 1 & 1 & 0 \\ 0 & 0 & 1 & 1 \\ 1 & 0 & 0 & 1 \end{bmatrix} \begin{bmatrix} x_{\Re}(t_1, t_2) \\ x_{\Re}(t_2, -t_1) \\ x_{\Re}(-t_1, -t_2) \\ x_{\Re}(-t_2, t_1) \end{bmatrix}.$$

The matrix of 1s and 0s is singular with rank three. We therefore have a redundancy. For example,

$$z(-t_2, t_1) = z(t_1, t_2) - z(t_2, -t_1) + z(-t_1, -t_2).$$

Any given sample can then be found from a linear combination of three other samples. One possible sampling geometry is shown in Fig. 14. Samples in the lighter yellow region can be calculated by samples in the darker green region and therefore need not be stored.

The sampling density for the rectangular grid is $SD = 1/(2W)^2$. The sampling geometry for the conjugate puzzle as exemplified in Fig. 14 reduces the sampling density $3SD/4$ real numbers per unit area. For the nonconjugated example, each sample is complex and the sampling density is $2SD$ real numbers per unit interval. Sampling schemes of the type illustrated in Fig. 13 reduce the number of samples by a factor

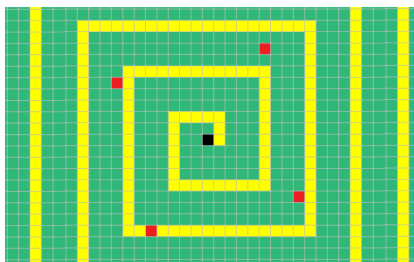


Fig. 14. Samples in the light yellow region can be found from a linear combination of three other samples. The three red boxes show four samples. The sample in any one of the red boxes can be found from a linear combination of the other three.

of $1/4$. The overall density is therefore $SD/2$ real numbers per unit interval. This is a lower density than the conjugate case.

8. THREEFOLD SYMMETRY SUBTILES

Threefold symmetric subtile periodicity is illustrated in the art of M. C. Escher, as shown in Fig. 15. Here we curiously can apply wordplay that Escher’s reptiles are subtiles. Three identical reptile subtile shapes related by $\pm 120^\circ$ form a strangely shaped tile able to periodically fill the plane without gaps.

Another example of threefold symmetry is illustrated in Fig. 16. Shown is a hexagon with an apothem of W . As shown, the hexagon is divided into three subtiles. The signal $X(\vec{u})$ is confined to the lightly shaded irregular hexagon on top. The origin is in the centroid of the hexagon. The spectrum $X(\vec{u})$ is rotated twice, once by -120° and then by $+120^\circ$, to form the two spectra $X(\mathbf{R}_{\pm 120^\circ})$, where the rotation matrices are

$$\mathbf{R}_{\pm 120^\circ} = \begin{bmatrix} \cos 120^\circ & \pm \sin 120^\circ \\ \mp \sin 120^\circ & \cos 120^\circ \end{bmatrix} = \frac{1}{2} \begin{bmatrix} -1 & \pm \sqrt{3} \\ \mp \sqrt{3} & -1 \end{bmatrix}.$$

The composite spectra shown in Fig. 16 fill the hexagon and can be written as

$$Y(\vec{u}) = X(\vec{u}) + X(\mathbf{R}_{-120^\circ}\vec{u}) + X(\mathbf{R}_{120^\circ}\vec{u}).$$

Because of the threefold symmetry, only a third of the samples corresponding to \mathbf{Q} need to be stored. Example sampling geometries are shown in Figs. 17 and 18. Samples are taken

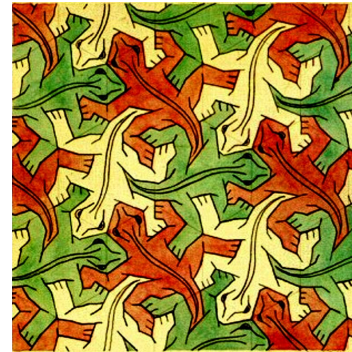


Fig. 15. Threefold subtile symmetry in the art of M. C. Escher [19]. To characterize only using rotation, the origin can be chosen at the point where the three left rear legs meet at the rightmost tip of the right toe.

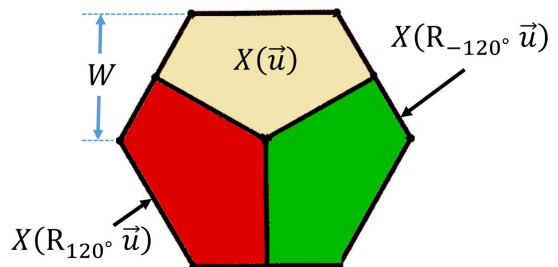


Fig. 16. Hexagon divided into three subtiles. The spectrum $X(\vec{u})$ is constrained to be in the top subtile. The spectrum $X(\vec{u})$ is rotated by $\pm 120^\circ$ to fill out the hexagonal support.

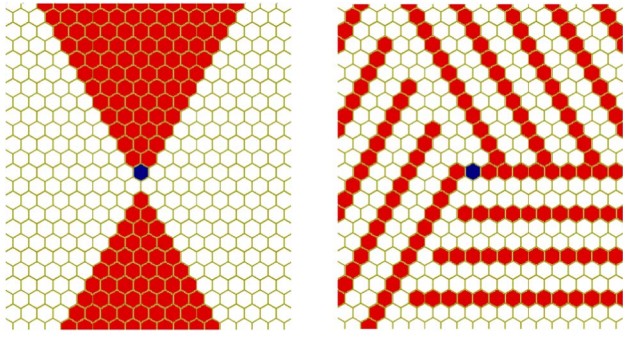


Fig. 17. Possible sampling geometries for the threefold symmetry of the spectrum shown in Fig. 16. Samples are taken at the center of each hexagon. Only samples in the red region are needed. Other samples are obtained by $\pm 120^\circ$ rotations.

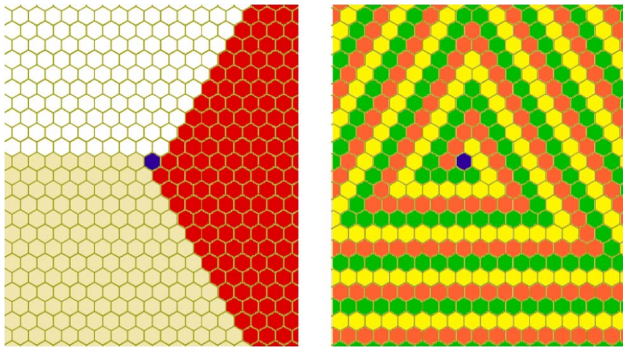


Fig. 18. More examples of sample locations for threefold symmetry. Any set of samples in any shaded area suffices to characterize the samples of the entire plane.

at the center of each hexagon, and the black hexagon denotes the origin. To obtain all the samples of y , the values of these samples are rotated $\pm 120^\circ$ to determine every sample in the plane.

The periodicity matrix for the regular hexagon is given in Eq. (6). The overlapping of sample locations on the hexagonal grid is geometrically obvious but can be confirmed using Eq. (16). Use the sampling matrix in Eq. (7) and the periodic matrix in Eq. (6). The sample locations overlap because the matrices

$$\mathbf{M}_{120^\circ} = \mathbf{P}^T \mathbf{R}_{120^\circ} \mathbf{Q} = \begin{bmatrix} 0 & 1 \\ -1 & -1 \end{bmatrix}$$

and

$$\mathbf{M}_{-120^\circ} = \mathbf{P}^T \mathbf{R}_{-120^\circ} \mathbf{Q} = \begin{bmatrix} -1 & -1 \\ 1 & 0 \end{bmatrix}$$

contain only integers.

Define the region \mathcal{S} as the irregular hexagon subtile in Fig. 16 where $X(\vec{u})$ resides. Interpolation then follows from Eq. (10) where the interpolation function is given by Eq. (12). Since the periodicity matrix \mathbf{P} for the regular hexagon is given in Eq. (6), we use

$$|\det \mathbf{Q}| = \frac{1}{|\det \mathbf{P}|} = \frac{1}{2\sqrt{3}W^2}. \tag{33}$$

9. SIXFOLD SYMMETRY

Six copies of the kite-shaped subtile in Fig. 19 form a hexagon. The subtiles are rotated $\pm 60^\circ$, $\pm 120^\circ$, and 180° . The $\pm 60^\circ$ rotation matrices are

$$\mathbf{R}_{\pm 60^\circ} = \frac{1}{2} \begin{bmatrix} 1 & \pm\sqrt{3} \\ \mp\sqrt{3} & 1 \end{bmatrix}.$$

The 180° rotation matrix is the negative of the identity matrix. All of these rotations give an \mathbf{M} matrix of integers. For example,

$$\mathbf{M}_{60^\circ} = \mathbf{P}^T \mathbf{R}_{60^\circ} \mathbf{Q} = \begin{bmatrix} 1 & 1 \\ -1 & 0 \end{bmatrix}$$

and

$$\mathbf{M}_{-60^\circ} = \mathbf{P}^T \mathbf{R}_{-60^\circ} \mathbf{Q} = \begin{bmatrix} 0 & -1 \\ 1 & 1 \end{bmatrix}.$$

The samples of all the rotated subtiles therefore will overlap.

A. Rotation

The combined rotations have a spectrum inside the hexagon of

$$Y(\vec{u}) = X(\vec{u}) + X(\mathbf{R}_{60^\circ}\vec{u}) + X(\mathbf{R}_{-60^\circ}\vec{u}) + X(\mathbf{R}_{120^\circ}\vec{u}) + X(\mathbf{R}_{-120^\circ}\vec{u}) + X(-\vec{u}). \tag{34}$$

The signal $y(\vec{t})$ containing superposition of six rotations of $x(\vec{t})$ therefore has the sixfold symmetry:

$$y(\vec{t}) = y(\mathbf{R}_{60^\circ}\vec{t}) = y(\mathbf{R}_{-60^\circ}\vec{t}) = y(\mathbf{R}_{120^\circ}\vec{t}) = y(\mathbf{R}_{-120^\circ}\vec{t}) = y(-\vec{t}).$$

Only one-sixth of the samples are required. Two possible sampling geometries are shown in Fig. 20.

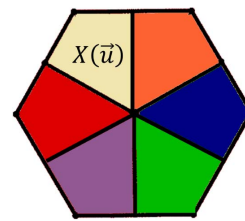


Fig. 19. Six kite-shaped subtiles form a hexagon.

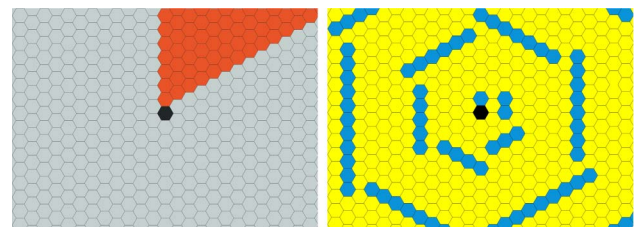


Fig. 20. Two possible sampling geometries for sixfold symmetry. The left shows a broken pie slice. On the right is a broken spiral.

B. Conjugation

The samples taken in the case above are complex. The same sampling density can be achieved with real samples if the rotations are appropriately conjugated to give a composite real image. In lieu of Eq. (34), let

$$Z(\vec{u}) = [X(\vec{u}) + X^*(-\vec{u})] + [X(\mathbf{R}_{120^\circ}\vec{u}) + X^*(\mathbf{R}_{-60^\circ}\vec{u})] + [X(\mathbf{R}_{-120^\circ}\vec{u}) + X^*(\mathbf{R}_{60^\circ}\vec{u})]. \quad (35)$$

The six spectrum components are shown here as three bracketed doublet terms. The terms are paired so that a kite is accompanied by the conjugate of its point symmetric reflection. Since there is conjugate symmetry,

$$Z(\vec{u}) = Z^*(-\vec{u}),$$

we are assured that $z(\vec{t})$ is real. Using Eq. (24) and Eq. (3),

$$z(\vec{t}) = 2[x_{\mathfrak{R}}(\vec{t}) + x_{\mathfrak{R}}(\mathbf{R}_{120^\circ}\vec{t}) + x_{\mathfrak{R}}(\mathbf{R}_{-120^\circ}\vec{t})].$$

The signal $z(\vec{t})$ has threefold symmetry:

$$z_{\mathfrak{R}}(\vec{t}) = z_{\mathfrak{R}}(\mathbf{R}_{120^\circ}\vec{t}) = z_{\mathfrak{R}}(\mathbf{R}_{-120^\circ}\vec{t}).$$

Thus only a third of the (real) samples need be taken. The sampling geometries in Figs. 17 and 18 are examples of sampling strategies applicable for this case.

C. Interpolation

The sampled images in Sections 9.A and 9.B are both regained by restoring values to the empty sample locations and using the formula in Eq. (10), where \mathcal{S} is the kite-shaped region labeled $X(\vec{u})$ in Fig. 19. The value of $|\det \mathbf{Q}|$ is in Eq. (33).

10. CONCLUSIONS

Images with support contained in subtiles can be used to reduce the density of stored samples required to characterize an image. We have analyzed twofold subtile symmetry for the cases of point reflection symmetry and mirror symmetry. The overall sampling density is shown to be reduced to the area of the subtile, which is half of conventional Nyquist sampling density. Threefold, fourfold, and sixfold subtile symmetry were similarly shown to reduce the sampling density by a third, a fourth, and a sixth.

A. Notes

Here are some takeaways.

As illustrated in Eq. (25), subtile sampling can allow real samples to represent complex images.

When analyzing the support of an image's spectrum, conventional analysis, by default, goes to the best fitting tile when considering sampling options. Such an approach gives rise to oversampling replications, as illustrated in Fig. 4. With the methodology presented, fitting the best subtile rather than the best tile to the image spectral support is now an option.

Subtile sampling theory is not as general as the PMC approach, but is more easily applied when applicable.

We also note that so-called *compressed sampling*, claiming effective sampling techniques below the Nyquist density, have been proposed but questioned [20].

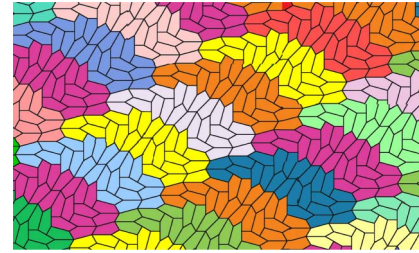


Fig. 21. Twenty-four identically shaped pentagon subtiles form a single tile [27].

B. Generalization

The analysis of subtile sampling we present is far from complete. We have presented no overarching theory but have only demonstrated application to specific cases. Even the cases discussed are not exhaustively examined. What happens in Fig. 19 when the kite immediately to the right of the kite labeled $X(\vec{u}) = X(u_1, u_2)$ is characterized by the transposition $X(-u_1, u_2)$ rather than a rotation $X(\mathbf{R}_{-60^\circ}\vec{u})$? And what if this transposition were conjugated? Likewise, we have considered only the case of subtile rotation. The approach can be extended to cases where there is both subtile rotation and translation.

The rotations considered herein are constrained to cases where subtile rotation corresponds to sample location rotation where the original and rotated samples coincide. Is there a generalization where the samples need not coincide? Of mathematical interest is pentagon tiling in response to Hilbert's 18th problem [21]. Reinhardt, in 1918, discovered five classes of pentagons that tile the plane [22]. Kershner found three more in 1968 [23]. Richard James found another in 1975 [24]. Amateur mathematician Marjorie Rice added another [25,26]. Using a computer search, Mann *et al.* recently discovered the 15th pentagon tiling solution [27,28]. Their tiling is shown in Fig. 21, where a tile is composed of 24 identically shaped subtiles. Rotations and translations of subtiles in such cases do not produce sample locations that coincide. Is there a generalization of the proposed subtile sampling applicable here?

REFERENCES AND NOTES

1. The Ed & Ray image in Fig. 1 does not conform to these properties and is used here for purposes of illustration only.
2. R. J. Marks II, "Ed & Ray Hersman in WWII," 2015, <https://marksmannet.com/RobertMarks/ArticlesAndEssays/EdRayHersmanWWII.pdf>.
3. R. J. Marks II, "Multidimensional signal sample dependency at Nyquist densities," *J. Opt. Soc. Am. A* **3**, 268–273 (1986).
4. M. A. Prelee and D. L. Neuhoff, "Multidimensional Manhattan sampling and reconstruction," *IEEE Trans. Inform. Theory* **62**, 2772–2787 (2016).
5. D. E. Dudgeon and R. M. Mersereau, *Multidimensional Digital Signal Processing*, Prentice-Hall Signal Processing Series (Prentice-Hall, 1984).
6. R. J. Marks II, *Handbook of Fourier Analysis & Its Applications* (Oxford University, 2009).
7. R. J. Marks II, *Introduction to Shannon Sampling and Interpolation Theory* (Springer, 2012).
8. A. Feldster, Y. P. Shapira, M. Horowitz, A. Rosenthal, S. Zach, and L. Singer, "Optical under-sampling and reconstruction of several

- bandwidth-limited signals," *J. Lightwave Technol.* **27**, 1027–1033 (2009).
9. R. J. Marks II and M. Hall, "Differintegral interpolation from a bandlimited signal's samples," *IEEE Trans. Acoust. Speech Signal Process.* **29**, 872–877 (1981).
 10. C.-C. Wei, H.-C. Liu, C.-T. Lin, and S. Chi, "Analog-to-digital conversion using sub-Nyquist sampling rate in flexible delay-division multiplexing OFDMA PONs," *J. Lightwave Technol.* **34**, 2381–2390 (2016).
 11. K. F. Cheung and R. J. Marks II, "Papoulis' generalization of the sampling theorem in higher dimensions and its application to sample density reduction," in *Proceedings of International Conference on Circuits and Systems*, Nanjing, China, July 6–8, 1989.
 12. K. F. Cheung, M. C. Poon, and R. J. Marks II, "A multidimensional extension of Papoulis' sampling expansion and some applications," in *Proceedings of the 1989 International Symposium on Computer Architecture and Digital Signal Processing* (Hong Kong, 1989), pp. 267–272.
 13. K. F. Cheung and R. J. Marks II, "Image sampling below the Nyquist density without aliasing," *J. Opt. Soc. Am. A* **7**, 92–105 (1990).
 14. C. Herley and P. W. Wong, "Minimum rate sampling and reconstruction of signals with arbitrary frequency support," *IEEE Trans. Inf. Theory* **45**, 1555–1564 (1999).
 15. J. W. Goodman, *Introduction to Fourier Optics* (Roberts, 2005).
 16. R. Solimene, M. A. Maisto, and R. Pierri, "Sampling approach for singular system computation of a radiation operator," *J. Opt. Soc. Am. A* **36**, 353–361 (2019).
 17. As is the case in Fig. 1, neither the Ed & Ray nor the Toes images conforms to these properties. They are used here for purposes of illustration only.
 18. A converse analysis answers a common sampling theorem question concerning real signals. If a one-dimensional signal is real, its Fourier transform is conjugately symmetric. Since knowing the spectrum for positive frequencies defines the negative frequencies, why not discard the negative frequency component of the signal and sample the signal corresponding to only the positive frequencies? The bandwidth will be half, therefore halving the sampling rate. The lower sampling frequency, however, results in complex samples. Two numbers for each sample are required for each sample. The original real signal has real samples. Thus, in terms of counting the required numbers per unit area, both sampling densities are the same.
 19. M. C. Escher, "Study of regular division of the plane with reptiles (1939)," By Source (WP:NFC#4), Fair use, <https://en.wikipedia.org/w/index.php?curid=48459647>.
 20. L. P. Yaroslavsky, "Can compressed sensing beat the Nyquist sampling rate?" *Opt. Eng.* **54**, 079701 (2015).
 21. V. McGlone, "The honors class: Hilbert's problems and their solvers," *Math. Intelligencer* **95**, 553 (2002).
 22. B. Grünbaum and G. C. Shephard, "Tilings with congruent tiles," *Bull. Am. Math. Soc.* **3**(3), 951–974 (1980).
 23. R. B. Kershner, "On paving the plane," *Am. Math. Monthly* **75**(8), 839–844 (1968).
 24. R. James, "New pentagonal tiling reported by Martin Gardner," *Sci. Am.* **1975**, 117–118 (1975).
 25. D. Schattschneider, "Tiling the plane with congruent pentagons," *Math. Mag.* **51**(1), 29–44 (1978).
 26. D. Singmaster and J. Zeitlin, "News and letters," *Math. Mag.* **30**(1), 308–312 (1985).
 27. C. Mann, J. McLoud-Mann, and D. Von Derau, "Convex pentagons that admit i-block transitive tilings," *Geom. Dedicata* **194**, 141–167 (2018).
 28. "The first new mathematical tile in 30 years is discovered," 2015, <https://blog.adafruit.com/2015/08/23/the-first-new-mathematical-tile-in-30-years-is-discovered/>.